LA-UR-16-21660 (Accepted Manuscript)

The role of disk self-gravity on gap formation of the HL Tau proto-planetary disk

Li, Shengtai
Li, Hui

To be published in: Journal of Physics: Conference Series

DOI to publisher's version: 10.1088/1742-6596/719/1/012007

Permalink to record: http://permalink.lanl.gov/object/view?what=info:lanl-repo/lareport/LA-UR-16-21660

The role of disk self-gravity on gap formation of the HL Tau proto-planetary disk

2016 J. Phys.: Conf. Ser. 719 012007

(http://iopscience.iop.org/1742-6596/719/1/012007)

The role of disk self-gravity on gap formation of the HL Tau proto-planetary disk

Shengtai Li and Hui Li
Theoretical Division, Los Alamos National Laboratory, Los Alamos, NM 87545, United States
E-mail: sli@lanl.gov

Abstract. We use extensive global hydrodynamic disk gas+dust simulations with embedded planets to model the dust ring and gap structures in the HL Tau protoplanetary disk observed with the Atacama Large Millimeter/Submillimeter Array (ALMA). Since the HL Tau is a relatively massive disk, we find the disk self-gravity (DSG) plays an important role in the gap formation induced by the planets. Our simulation results demonstrate that DSG is necessary in explaining of the dust ring and gap in HL Tau disk. The comparison of simulation results shows that the dust rings and gap structures are more evident when the fully 2D DSG (non-axisymmetric components are included) is used than if 1D axisymmetric DSG (only the axisymetric component is included) is used, or the disk self-gravity is not considered. We also find that the couple dust+gas+planet simulations are required because the gap and ring structure is different between dust and gas surface density.

1. Introduction

ALMA observations of HL Tau, a young ($\leq$ 1-2 Myr) star in Taurus, revealed bright and dark rings in the millimeter-wave continuum emission [1]. One interesting question is whether these structures are created by the embedded planets, hence yielding potentially important clues on planet formation in such disks.

Some observational features suggest however that the pattern of rings shown in HL Tau disk may be produced by planets. First, the spectral index derived from the ALMA images suggests that the dark rings are optical thin whereas the bright regions are optically thick, therefore the dark rings are real gaps in the dust distribution [1]. Second, the increase of the eccentricity of the rings at large orbital radii [1] is consistent with the fact that the orbital eccentricities of exoplanets increase with orbital radii [2, 3, 4]. Third, the dust size constrained by the polarized emission is around 150 μm [5], which means the structure of multiple rings should also exist in the gas disk because dust at this size should be well coupled with gas.

Models of disks that couple the dynamics of gas, dust and planets are crucial to interpret the observed patterns in the HL Tau system [6, 7, 8]. Various models suggest that the disk mass of HL Tau is $\sim$ 0.03-0.14 $M_\odot$ [9, 10, 11, 12], and the estimated stellar mass of HL Tau is 0.55 to 1.3 $M_\odot$ [13, 14, 15, 1]. The high disk mass might affect the disk stability and the resonance locations of potential planets [16]. A recent study by [8] used a two-fluid SPH code that includes gas+dust disk and embedded planets. Though they were able to reproduce the pattern of bright and dark rings, they adopted a disk mass of only 0.0002 $M_\odot$ within 120 AU and under predicted by about a factor 20 the observed millimeter flux density. The disk self-gravity (DSG) is not included in their simulations because it is not important with such a low disk mass.

We have run extensive global hydrodynamic disk gas+dust simulations with embedded planets, coupled with three dimensional radiative transfer calculations, to model the dust ring and gap structures in the HL Tau disk. We have performed quantitative fitting to the ALMA observations of HL Tau in terms of its millimeter flux density and spatial variations in [17]. In this paper, we use our 2D numerical simulations to demonstrate the important of the disk self-gravity in the gap formation if the proto-planet is present in HL Tau disk. We describe our approach and model set-up in Section 2 and our numerical method and code in Section 3. We then show our main results in Section 4 and discuss their implications in Section 5.

2. Numerical model and initial setup

We adopt a disk model from [11]. The disk surface density is described by

$$\Sigma_g(r) = \Sigma_0 \Big(\frac{r}{r_0}\Big)^{0.23} \exp[-(r/r_c)^{2.23}] \quad , \tag{1}$$

where $r_c = 79$ AU is a characteristic radius [18] and $r_0 = 10$ AU. The mass of the star is $M_* = 0.55 M_\odot$. The locally isothermal sound speed is chosen as:

$$\Big(\frac{c_s}{v_\phi}\Big)(r) = 0.05 \Big(\frac{r}{r_0}\Big)^{0.285} \quad . \tag{2}$$

which implies the disk temperature varies as $T \propto T_0 (r/r_0)^{-0.43}$. The whole disk is assumed to have a constant Shakura-Sunyaev viscosity parameter $\alpha = 10^{-3}$. The ratio of the scale height to the radius, $H/r(r_0) = 0.05$ (see Eq. (2), is adopted for gas after extensive experiments to fit the simulation data to the observation data. The value of H/r for dust particles is different for different particle sizes when we calculate the disk temperature and vertical distribution of the dust profile (see [17] for more details).

Although Kwon et al. [11] finds a disk mass of $0.135 M_\odot$, we find that the disk with this mass quickly becomes gravitationally unstable under small perturbations. Hence we reduce the disk mass to be $M_{\rm disk} \approx 7.35 \times 10^{-2}\ M_\odot$, which leads to $\Sigma_0 = 4.83 \times 10^{-4} [M_*/(10{\rm AU})^2] \approx 23.61$ g/cm^2. With these given parameters, we can estimate the Toomre's Q-parameter (see Fig. 1). Initially it has the minimum value of ~ 1.61, and we expect the disk self-gravity plays important role with this low Q-value.

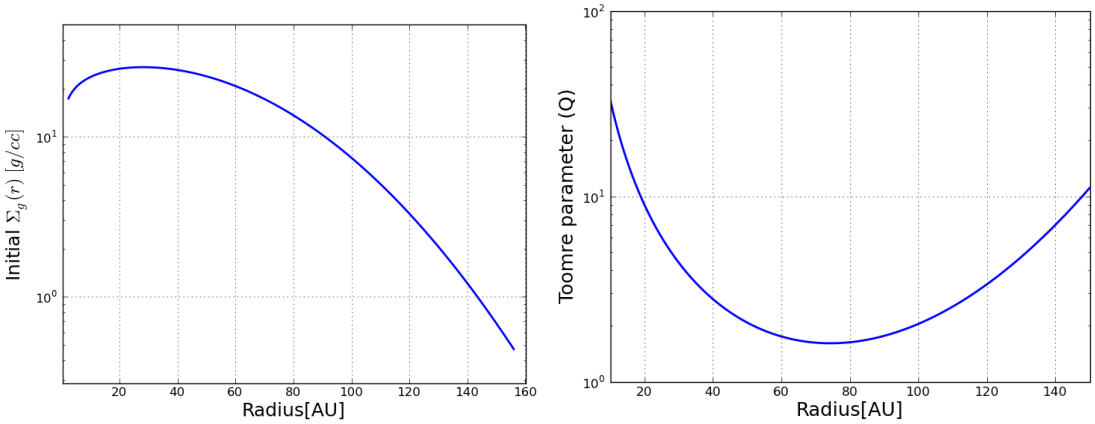

Figure 1. Initial disk surface density of the gas (Σ_g) and Toomre's Q-parameter.

We adopt dust grains with a size of 0.15 mm as best tracers of the dust emission at 1 mm. This is because single grain opacities were averaged on a grain size distribution to obtain the mean

opacity used in the radiative transfer model, and the resulting dust opacity at the wavelength of 1 mm is dominated by dust grains with sizes between 0.1 and 0.2 mm.

ALMA Partnership et al. [1] identify seven pairs of dark and bright rings in the 1.0 mm image of the HL Tau disk, and among them four prominent dark rings could be considered as gaps, i.e., the dark rings D1, D2, and the adjoining D5 and D6. Based on a large body of previous literature on gap opening and formation as functions of disk gas temperature, planet mass, disk viscosity [19, 20], we have performed tens of disk+planet hydro simulations in order to determine the likely planet mass values that could roughly match the multiple gap widths and depths as shown in the ALMA observations. Based on these simulations, we adopt a set of planet mass parameters as $M_p \approx 0.35, 0.17$, and $0.26 M_{\rm Jup}$ at $13.1, 33.0$, and 68.6 AU, respectively. These three planets are fixed at their orbital locations, and planetary radial migration is turned off.

3. Numerical method

We solve the 2D disk model using LA-COMPASS code [21, 20, 22] to simulate the planet-disk interaction. The disk is treated as a 2D self-gravitating gas, whose motion is described by the Navier-Stokes equations, coupled to a similar (pressure-less) system of equations for the dust in a polar coordinate $\{r, \phi\}$ centered on the star. The dust particles are treated as pressure-less fluid. The two sets of equations for gas and dust particles are coupled via drag terms. A second-order high-resolution Godunov scheme is used to solve the equations numerically with exact Riemann solver for gas and dust. The planet motion is subject to the Newton's law with the gravitational force from the central star, other planets, and the disk material. The coupling between the disk and planet motions is carefully considered. For the small dust particles, we use a multiscale approach to accelerate the time integration. We also include the diffusion transport to the dust due to the turbulent motion of the gas. The momentum equations for the dust are modified to be consistent with the diffusion transport in the continuity equation. A fast disk self-gravity (DSG) solver is developed using the approach described in [23]. The indirect acceleration term due to the force exerted by the disk material on the star is also included together with the DSG solver without extra effort. The code is fully parallelized via message-passing interface coupled with OpenMP for multi-threads.

For numerical simulations, we have to impose the disk boundary $r \in [r_{\rm min}, r_{\rm max}]$. We adopt a value $r_{\rm min} = 2.4$AU from [11]. We use $r_{\rm max} = 156$AU. We have also tried other values of $r_{\rm min}$ and $r_{\rm max}$ and found that it does not make big difference in our simulations. A fixed boundary condition is used for gas at both inner and outer disk boundaries. For dust, we adopt an inflow (outflow) boundary condition at the inner (outer) boundary.

For the DSG calculation, we also include the disk material in the inner disk between 0.1AU and 2.4AU, and the outer disk between 156AU and 1560AU. Both the inner disk and outer disk are assumed to be fixed as the initial setup during the whole simulations. This approach avoids the sharp variation in the DSG near the $r_{\rm min}$ and $r_{\rm max}$.

For comparison, we also include the numerical results of 1D axisymmetric DSG solver [24].

4. Numerical result

The disk is discretized by 3072×768 grid in (r, ϕ) domain. We run the simulation up to 7000 orbits (measured at $r_0 = 10$AU). We find the disk surface variation becomes very small at later stage.

Fig. 2 shows the disk surface density of the gas component (Σ_g) between different disk self-gravity setup and at different times. We compare three different simulations: with fully 2D DSG, with only 1D axis-symmetric DSG, and without DSG (i.e., disk self-gravity is not considered). We plot the variation of Σ_g from 1000 orbits to 4000 orbits. It is clear that the one-dimensional axis-symmetric DSG (DSG1D in the plot) generates similar results as the case without DSG. However the fully 2D DSG generate a clearer and deeper gap at later times than the case without

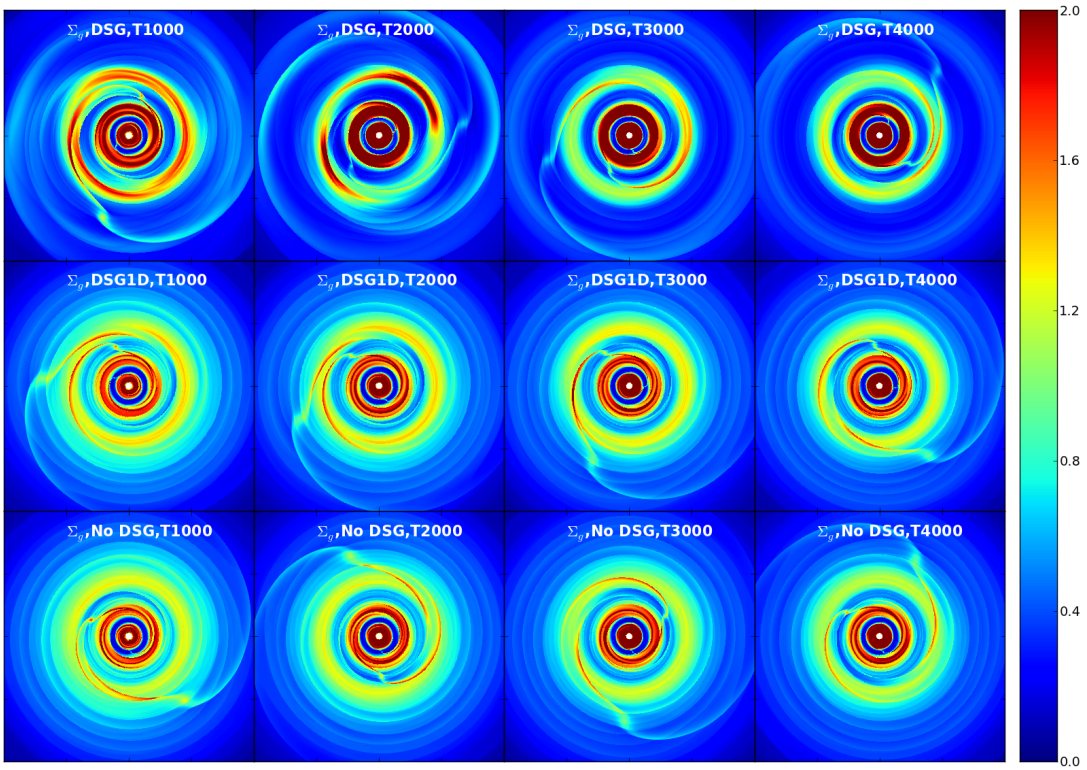

Figure 2. Disk surface density of the gas (Σ_g) at different times and between different disk self-gravity (DSG) setup. The time is represented by the orbits at 10AU radius.

DSG. This shows that the non-axisymmetric components of the disk self-gravity is important even though the disk looks axisymmetric.

An interesting feature shown in the Fig. 2 is the case at T=2000 orbits and with DSG turned on. The disk becomes slightly eccentric at this time shown by the two high density blobs near the edge of the second gap. This eccentricity eventually gets damped with the time evolution and totally disappear when the time reaches T=4000 orbits. We notice that the eccentric disk is caused mainly by both the indirect acceleration term due to the force exerted by the disk material on the star and the disk self-gravity. If we turn off this indirect acceleration term or turn off the DSG, the disk will not become eccentric. We remark that this is not purely a numerical issue as we have verified it using FARGO code and obtained similar eccentric disk. More results on this feature will be reported in the future.

Fig. 3 shows the disk surface density for the dust components. It is clear the gap become more outstanding in the dust surface density than in the gas surface density if the DSG is used. If no DSG or 1D-DSG is used, the outer ring and gap is barely visible.This shows the importance of the DSG in the gap formation, especially for the outer gap and dust ring.

Comparing Fig. 3 and Fig. 2, we find the axis-symmetric structure of the gap and dust ring is more evident in the dust surface plots than the gas surface plots. Also the spiral arms in the gas plots disappear in the dust plots. This can partially explain why the spiral arm is not visible in the observation images of ALMA.

Fig. 4 shows the azimuthal-average quantity at $t = 4000$ orbits. It is clear that the gap is much deeper and the gap edge is much higher if the DSG is used. We also plot the dust-to-gas ratio Σ_d/Σ_g. Initially, $\Sigma_d/\Sigma_g = 0.01$. Most simulation models that do not include dust dynamics

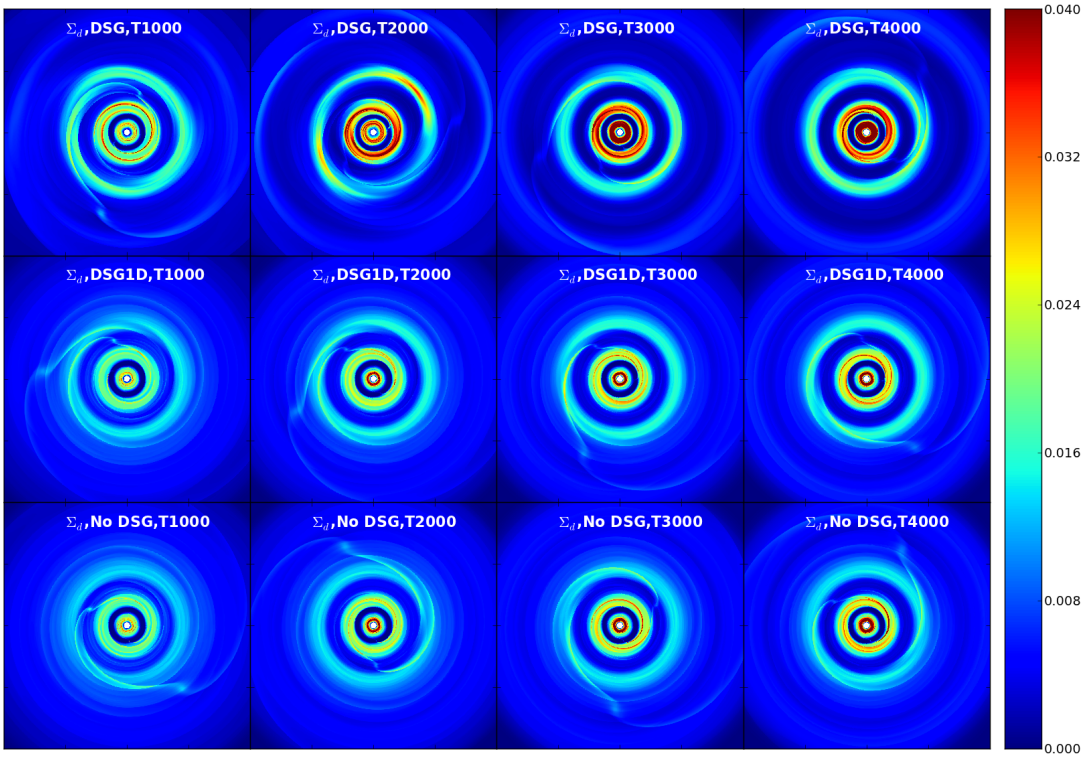

Figure 3. Disk surface density of the dust component (Σ_d) at different times and between different disk self-gravity (DSG) setup. The time is represented by the orbits at 10AU radius.

assume this ratio remains fix during the whole simulation. However, the right plot of the Fig. 4 shows this ratio can be changed dramatically in the gap region: near the bottom of the gap, $\Sigma_d/\Sigma_g \approx 0.005$; at the gap edge, $\Sigma_d/\Sigma_g \approx 0.02$; a factor of 4 variation.

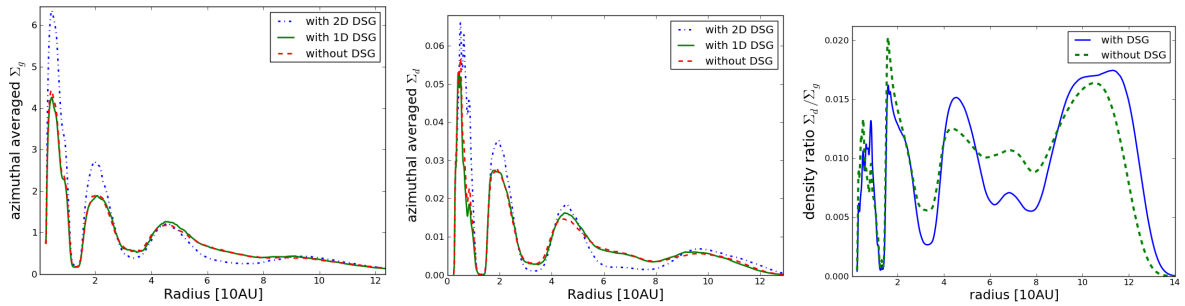

Figure 4. Azimuthal-averaged surface density for gas and dust at time T=4000 orbits. The right plot shows the azimuthal averaged dust-to-gas ratio (Σ_d/Σ_g)at T=4000 orbits

5. Conclusion

We have proposed a model to simulate the observed feature in the HL Tau disk. Our simulations show that the disk self-gravity (DSG) plays an important role in the gap formation. Without DSG, the outer gap and dust rings is barely visible and cannot be fit with the observed data.

We also show that the simplified axis-symmetric 1D DSG does not help even if it is included in the simulations.

Our simulations also show that we cannot simply use the results of gas surface density to derive the dust distribution as conventional approach does. The dust-to-gas ratio can be changed dramatically near the gap and cannot be kept as constant. The fully coupled dust+gas+planet simulation is necessary.

Acknowledgments

This research was performed under the auspices of the Department of Energy. It was supported by the Laboratory Directed Research and Development (LDRD) Program at Los Alamos.

References

[1] Partnership A, Brogan C L, Perez L and et al 2015 *ApJL* **808** L3
[2] Butler R, Wright J, Marcy G and et al 2006 *ApJ* **646** 505
[3] Shen Y and Turner E L 2008 *ApJ* **685** 553
[4] Zhang X, Li H, Li S and Lin D 2014 *ApJL* **789** L23
[5] Kataoka A, Muto T, Momose M, Tsukagoshi T and Dullemond C 2015 arXiv:1507.08902
[6] Dong R, Zhu Z and Whitney B 2014 arXiv:1411.6063
[7] Zhu Z, Stone J and Bai X 2015 *ApJ* **801** 81
[8] Dipierro G, Price D, Laibe G and et al 2015 *MNRAS* **453** L73–L77
[9] Robitaille T, Whitney B A, Indebetouw R and Wood K 2007 *ApJS* **169** 328
[10] Guilloteau S, Dutrey A, Piétu V and Boehler Y 2011 *A&A* **529** A105
[11] kwon W, Looney L and Mundy L 2011 *ApJ* **741** 3
[12] kwon W, Looney L, Mundy L and Welch W 2015 *ApJ* **808** 102
[13] Sargent A I and Beckwith S V W 1991 *ApJL* **382** L31
[14] Close L M, Roddier F, Hora J L and et al 1997 *ApJ* **489** 210
[15] White R and Hillenbrand L 2004 *ApJ* **616** 998
[16] Tamayo D, Triaud A, Menou K and Rein H 2015 *ApJ* **805** 100
[17] Jin S, Li S, Li H and et al 2016 *ApJ* **818** 76
[18] Andrews S M and et al 2009 *ApJ* **700** 1502
[19] Crida A, Morbidelli A and Masset F 2006 *ICARUS* **181** 587
[20] Li H, Li S, Lubow S H and Lin D 2009 *ApJL* **690** L52–L55
[21] Li H and et al 2005 *ApJ* **624** 1003
[22] Fu W, Li H, and S Li S L and Liang E 2014 *ApJL* **795** L39
[23] Li S, Buoni M and Li H 2009 *ApJ* **181** 244–254
[24] Huré J M 2005 *A&A* **434** 17–23